TBPL2/TFIIA complex establishes the maternal transcriptome by an oocyte-specific promoter usage

Changwei Yu[1,2,3,4], Nevena Cvetesic[5], Vincent Hisler[1,2,3,4], Kapil Gupta[6], Tao Ye[1,2,3,4], Emese Gazdag[1,2,3,4], Luc Negroni[1,2,3,4], Petra Hajkova[5], Imre Berger[6], Boris Lenhard[5], Ferenc Müller[7], Stéphane D. Vincent[1,2,3,4,8,*] and László Tora[1,2,3,4,8,*]

[1]Institut de Génétique et de Biologie Moléculaire et Cellulaire, 67404 Illkirch, France;

[2]Centre National de la Recherche Scientifique (CNRS), UMR7104, 67404 Illkirch, France;

[3]Institut National de la Santé et de la Recherche Médicale (INSERM), U1258, 67404 Illkirch, France;

[4]Université de Strasbourg, 67404 Illkirch, France;

[5]Imperial College London, South Kensington Campus, London SW7 2AZ, UK;

[6]Max Planck Bristol Centre for Minimal Biology, University of Bristol, Cantock's Close, Bristol BS8 1TS, UK.

[7]Institute of Cancer and Genomic Sciences, College of Medical and Dental Sciences, University of Birmingham, UK;

[8] These authors contributed equally to this work

[*]Co-corresponding authors: S.D.V. vincent@igbmc.fr and L.T. laszlo@igbmc.fr

Abstract

During oocyte growth, transcription is required to create RNA and protein reserves to achieve maternal competence. During this period, the general transcription factor TATA binding protein (TBP) is replaced by its paralogue, TBPL2 (TBP2 or TRF3), which is essential for RNA polymerase II transcription. We show that in oocytes TBPL2 does not assemble into a canonical TFIID complex. Our transcript analyses demonstrate that TBPL2 mediates transcription of oocyte-expressed genes, including mRNA survey genes, as well as specific endogenous retroviral elements. Transcription start site (TSS) mapping indicates that TBPL2 has a strong preference for TATA-like motif in core promoters driving sharp TSS selection, in contrast with canonical TBP/TFIID-driven TATA-less promoters that have broader TSS architecture. Thus, we show a role for the TBPL2/TFIIA complex in the establishment of the oocyte transcriptome by using a specific TSS recognition code.

Introduction

Regulation of transcription initiation by RNA Polymerase II (Pol II) is central to all developmental processes. Pol II transcription requires the stepwise assembly of multi-protein complexes called general transcription factors (GTFs) and Pol II[1]. The evolutionary conserved TFIID complex plays a major role in transcription initiation as it is the first GTF to initiate the assembly of the pre-initiation complex (PIC) by recognizing the core promoter[2]. TFIID is a large multi-protein complex composed of the TATA box-binding protein (TBP) and 13 TBP-associated factors (TAFs) in metazoa[3]. The model suggesting that transcription is always regulated by the same transcription complexes has been challenged in metazoans by the discovery of cell-type specific complexes containing specialized GTF-, TBP- or TAF-paralogs[4]. Two TBP paralogues have been described in vertebrates: TBPL1 (TBP like factor; TLF, also known as TRF2) has been identified in all metazoan species[5-10], while TBPL2 (also known as TRF3 or TBP2) has only been described in vertebrates[11,12]. Remarkably, while *Tbpl1* and *Tbpl2* mutants display embryonic phenotypes in non-mammalian species[7-10,12,13], *Tbpl1* and *Tbpl2* loss of function in mouse results in male and female sterility, respectively[14-16], suggesting that in mammals, these two TBP-like proteins are involved in cell specific transcription. While TBPL2 shares high degree of identity (92%) within the conserved saddle-shaped C-terminal DNA binding core domain of TBP[17], the C-terminus of TBPL1 is more distant with only 42% identity[12]. A consequence is that TBPL2, but not TBPL1, is able to bind canonical TATA-box sequences *in vitro*[5,12,18]. The N-terminal domains of the three vertebrate TBP related factors do not show any conservation. All three vertebrate TBP related factors can interact with the GTFs TFIIA and TFIIB, and can mediate Pol II transcription initiation *in vitro*[12,13,18-20]. However, how alternative initiation complexes form, how they

63 regulate cell type-specific transcription and how they recognize promoter sequences remain
64 unknown.

65 Mapping of transcription start sites (TSSs), at single-nucleotide by Cap Analysis of
66 Gene Expression (CAGE) revealed two main modes for transcription start site (TSS) usage[21].
67 Transcription initiation within a narrow region, called "sharp" (or focused) TSS-type, is
68 common in highly active, tissue-specific gene promoters containing TATA boxes, while
69 transcription initiation with multiple initiation positions within an about 100 bp region, called
70 "broad" TSS promoter architecture[21], are more characteristic to ubiquitously expressed and
71 developmental regulated genes (reviewed in [22]). During zebrafish maternal to zygotic
72 transition it was described that two TSS-defining grammars coexist, in core promoters of
73 constitutively expressed genes to enable their expression in the two regulatory
74 environments[23]. Maternally active promoters in zebrafish tend to be sharp, with TATA-like,
75 AT-rich (W-box) upstream elements guiding TSS selection, while embryonically active broad
76 promoter architectures of the same genes appear to be regulated by nucleosome positioning
77 ques. Although a number of germ cell specific as well as somatic transcriptional regulators
78 have been well characterized during folliculogenesis (reviewed in [24]), the exact actors and
79 mechanisms required for setting up the oocyte specific transcriptome have not yet been
80 identified in vertebrates.

81 Female germ cells develop during oogenesis leading to the formation of a highly
82 differentiated and specialised cell, the oocyte. In females, oocytes enter meiosis during
83 embryonic life. Quiescent primordial follicles composed of meiotically arrested oocytes at the
84 late diplotene stage and surrounded by granulosa cells, are formed perinatally in mice
85 (reviewed in [24]). Shortly after birth, some primordial follicles enter folliculogenesis and
86 undertake a growth phase during which a specific oocyte-specific transcriptome is set up,
87 oocytes increase their size until the pre-antral follicular stage[25]. A remarkable feature of

88 oocyte is the very high expression of retrotransposons driven by Pol II transcription. These
89 elements are interspersed repetitive elements that can be mobile in the genome. One of the 3
90 major classes of retrotransposons in mammals is the long terminal repeat (LTR)
91 retrotransposons derived from retroviruses, also known as endogenous retroviruses (ERVs)
92 that is subdivided in 3 sub-classes: ERV1, ERVK and endogenous retrovirus like ERVL-
93 MaLR (mammalian apparent LTR retrotransposons) (reviewed in [26]). Transcription of mobile
94 elements in specific cell types depends on the presence of a competent promoter recognition
95 transcription machinery and/or the epigenetic status of the loci where these elements have
96 been incorporated. Remarkably, MaLRs encode no known proteins, but MaLR-dependent
97 transcription is key in initiating synchronous developmentally regulated transcription to
98 reprogram the oocyte genome during growth[27].

99 Remarkably, during oocyte growth TBP is absent and replaced by TBPL2[28]. Indeed,
100 TBP is only expressed up to the primordial follicular oocytes and becomes undetectable at all
101 subsequent stages during oocyte growth. In contrast, TBPL2 is highly expressed in the
102 growing oocytes, suggesting that TBPL2 is replacing TBP for its transcription initiating
103 functions during folliculogenesis[28]. In agreement with its oocyte-specific expression, a crucial
104 role of TBPL2 for oogenesis was demonstrated in *Tbpl2*$^{-/-}$ females, which show sterility due
105 to defect in secondary follicle production[16,29]. In the absence of TBPL2, immunofluorescent
106 staining experiments showed that elongating Pol II and histone H3K4me3 methylation signals
107 were abolished between the primary and secondary follicle stage oocytes suggesting that Pol
108 II transcription was impaired[16]. Initially TBPL2/TRF3 was suggested to be expressed during
109 muscle differentiation[30], but this observation was later invalidated[16,29]. Altogether, the
110 available data suggested that TBPL2 is playing a specialized role during mouse oocyte
111 development. However, how does TBPL2 regulate oocyte-specific transcription and what is
112 the composition of associated transcription machinery, remained unknown.

Here we demonstrate that in oocytes TBPL2 does not assemble into a canonical TFIID complex, while it stably associates with TFIIA. The observation that the oocyte specific deletion of *Taf7*, a TFIID specific TAF, does not influence oocyte growth and maturation, corroborates the lack of TFIID in growing oocytes. Our transcriptomics analyses in wild type and *Tbpl2*$^{-/-}$ oocytes show that TBPL2 mediates transcription of oocyte-expressed genes, including mRNA destabilisation factor genes, as well as MaLR ERVs. Our transcription start site (TSS) mapping from wild-type and *Tbpl2*$^{-/-}$ growing oocytes demonstrates that TBPL2 has a strong preference for TATA-like motif in gene core promoters driving specific sharp TSS selection. This is in marked contrast with TBP/TFIID-driven TATA-less gene promoters in preceding stages that have broad TSS architecture. Our results show a role for the TBPL2-TFIIA transcription machinery in a major transition of the oocyte transcriptome mirroring the maternal to zygotic transition that occurs after fertilization, completing a full germ line cycle.

Results

Oocyte-specific TBPL2/TFIIA complex distinct from TFIID

To characterize TBPL2-containing transcription complexes we prepared whole cell extracts (WCE) from growing 14 days post-natal (P14) mouse ovaries and analysed TBPL2-associated proteins by anti-mTBPL2 immunoprecipitation (IP) coupled to label free mass spectrometry (Fig. 1a, Supplementary Fig. 1a, b). To determine the stoichiometry of the composition of the immunoprecipitated complexes, normalized spectral abundance factor (NSAF) values were calculated[31]. In the anti-TBPL2 IPs we identified TFIIA-αβ and TFIIA-γ subunits as unique GTF subunits associated with TBPL2 (Fig. 1a, Supplementary Data 1). As ovaries contain many other non-oocyte cell types which express TBP, in parallel from the same extracts we carried out an anti-TBP IP. The mass spectrometry of the anti-TBP IP indicated that TBP assembles into the canonical TFIID complex in non-oocyte cells (Fig. 1b, Supplementary Data 2). As growing oocytes represent only a tiny minority of ovary cells, we further tested the TBPL2-TFIIA interaction by a triple IP strategy (Fig. 1c): first, we depleted TAF7-containing TFIID complexes with an anti-TAF7 IP, second, the remaining TFIID and SAGA complexes, which contain also shared TAFs[32], were depleted with an anti-TAF10 IP using the anti-TAF7 IP flow-through as an input, third we performed an anti-TBPL2 IP on the anti-TAF7/anti-TAF10 flow-through fraction (Fig. 1d-f, Supplementary Data 3). The analysis of this third consecutive IP further demonstrated that TBPL2 forms a unique complex with TFIIA-αβ, and TFIIFA-γ, but without any TFIID subunits.

To further analyse the requirement of TFIID during oocyte growth, we carried out a conditional depletion of TFIID-specific *Taf7* gene during oocyte growth using the *Zp3-Cre* transgenic line[33] (Supplementary Fig. 1c-g). Remarkably, TAF7 is only detected in the cytoplasm of growing oocyte (Supplementary Fig. 1c). The oocyte-specific deletion of *Taf7*

152 did not affect the presence of secondary and antral follicles and the numbers of collected
153 mature oocytes after superovulation (Fig. 1g, h, Supplementary Fig. 1f). The lack of
154 phenotype is not due to an inefficient deletion of *Taf7*, as TAF7 immunolocalization is
155 impaired (Supplementary Fig. 1d, e), and as oocyte-specific *Taf7* mutant females are severely
156 hypofertile (Supplementary Fig. 1g). The observations that TBP is not expressed in growing
157 oocytes, and that the oocyte specific deletion of *Taf7* abolishes the cytoplasmic localization of
158 TAF7, but does not influence oocyte growth, show that canonical TFIID does not assemble in
159 the nuclei of growing oocytes. Thus, our results together demonstrate that during oocyte
160 growth a stable TBPL2-TFIIA complex forms, and may function differently from
161 TBP/TFIID.

162 In order to further characterize the composition of the TBPL2-TFIIA complex, we
163 took advantage of NIH3T3 cells artificially overexpressing TBPL2 (NIH3T3-II10 cells[28]). In
164 this context where TBP and TAFs are present, TFIID is efficiently pulled down by an anti-
165 TBP IP, but no interaction with TFIIA could be detected (Fig. 2a). Interestingly, the anti-
166 TBPL2 IP showed that the artificially expressed TBPL2 can incorporate in TFIID-like
167 complexes as TAFs were co-IP-ed (Fig. 2a), however with much lower stoichiometry (NSAF
168 values) than that of TBP (Fig. 2b). In contrast, strong interaction with TFIIA-αβ and TFIIFA-
169 γ were detected, suggesting that the TBPL2-TFIIA complex can be formed in the NIH3T3-
170 II10 cells and that TBPL2, to the contrary to TBP has the intrinsic ability to interact with
171 TFIIA. Remarkably, in spite of the high similarity between the core domains of TBP and
172 TBPL2, no interaction with SL1 (TAF1A-D) and TFIIIB (BRF1) complexes that are involved
173 in Pol I and Pol III transcription, respectively[34]) could be detected in the anti-TBPL2 IP, to the
174 contrary to the anti-TBP IP in the NIH3T3-II10 (Fig. 2a, b) as well as in the ovary
175 (Supplementary Data 1, 2), suggesting that TBPL2 is not involved in Pol I and Pol III
176 transcription initiation in the growing oocytes.

To analyze whether TBPL2 associates with TFIID TAFs and TFIIA in the same complex, we performed a gel filtration analysis of NIH3T3-II10 WCE. The profile indicated that most of the TBPL2 and TFIIA could be found in the same fractions (22-26) eluting around 150-200 kDa, while TBPL2 protein was below the detection threshold of the western blot assay in the TAF6-containing fractions 9-15 (Fig. 2c). To verify that TBPL2 and TFIIA are part of a same complex in fractions 22-26, we IP-ed TBPL2 from these pooled fractions and subjected them to mass spectrometric analysis. Our data confirmed that in these fractions eluting around 170 kDa, TBPL2 and TFIIA form a stable complex that does not contain any TAFs (Fig. 2d, supplementary Data 4). Thus, all these experiments together demonstrate that TBPL2/TFIIA form a stable complex in oocytes, where TBP is not expressed and TBPL2/TFIIA is the only promoter recognizing transcription complex that could direct Pol II transcription initiation (see the summary of all these IPs in Fig. 2e).

TBPL2-dependent oocyte transcriptome

To characterize the growing oocyte-specific transcriptome and its dependence on TBPL2, we have performed a transcriptomic analysis of wild-type (WT) and *Tbpl2*$^{-/-}$ oocytes isolated from primary (P7) and secondary follicles and (P14) (Fig. 3, 4, Supplementary Fig. 2, Supplementary Data 5). We observed down-regulation of a high number of oocyte-specific genes, out of which *Bmp15* and *Gdf9* served as internal controls[35,36], as they were already described to be regulated by TBPL2[16] (Fig. 3a, b and Supplementary Fig. 2a). Principal component analysis showed that the four distinct RNA samples clustered in individual groups and that the main explanation for the variance is the genotype, and then the stage (Supplementary Fig. 2b). Comparison of the RNA level fold changes between mutant and WT oocytes showed that in *Tbpl2*$^{-/-}$, there is a massive down-regulation of the most highly expressed transcripts, both at P7 and P14 (Supplementary Fig. 2c). The Pearson correlation

202 between the P7 and P14 fold change data sets for transcripts expressed above 100 normalized
203 reads was close to 0.8 (Supplementary Fig. 2c), indicating that *Tbpl2* loss of function
204 similarly altered RNA levels at P7 and P14 stages. We therefore focused on the P14 stage for
205 the rest of the study.

206 In WT P14 oocytes transcripts corresponding to 10791 genes were detected.
207 Importantly, many of these detected transcripts have been transcribed at earlier stages and are
208 stored in growing oocytes[37]. As there is no Pol II transcription in *Tbpl2*$^{-/-}$ growing oocytes[16],
209 RNAs detected in the *Tbpl2*$^{-/-}$ mutant oocytes represent mRNAs transcribed by a TBP/TFIID-
210 dependent mechanism and deposited into the growing oocytes independently of TBPL2
211 activity at earlier stages, i.e. at primordial follicular stage, where TBP is still expressed. The
212 proportion of genes (1396) upregulated following *Tbpl2* deletion (Fig. 3c) can be explained
213 by two mutually not exclusive ways: i) the consequence of the normalization to the library
214 size resulting in a slight over-estimation of up-regulated transcripts, and ii) under-estimation
215 of down-regulated transcripts and/or by transcript buffering mechanisms due to mRNA
216 stabilization[38]. Validation of the up-regulation of some candidate transcripts levels
217 (Supplementary Fig. 2d, e) strongly supports the latter hypothesis (but see also the next
218 paragraph).

219 Nevertheless, we detected 1802 significantly downregulated transcripts in the *Tbpl2*$^{-/-}$
220 oocytes (Fig. 3c). Key genes known to be expressed during oocyte growth, such as *Bmp15,*
221 *Eloc, Fgf8, Gdf9* and *Zar1*[35,36,39], were confirmed by RT-qPCR to be down-regulated
222 (Supplementary Fig. 2f, g). These results suggest that TBPL2 has an important role in gene
223 expression in the growing oocytes. Gene Ontology (GO) analyses of biological process of the
224 identified down regulated categories of genes (Supplementary Data 6) indicated that many
225 genes, involved in meiosis II and distinct cell cycle processes, were significantly down-
226 regulated (Supplementary Fig. 2h). The most enriched molecular function GO category was

"poly(A)-specific ribonuclease activity" containing many genes coding for factors or subunits of complexes contributing to deadenylation/decapping/decay activity in eukaryotes (Fig. 3d) (i.e. CCR4-NOT, PAN2/PAN3[40]; DCP1A/DCP2[41], or BTG4[39]). In good agreement with the transcriptome analyses, transcripts coding for these "poly(A)-specific ribonuclease activity" factors were significantly down regulated in *Tbpl2*$^{-/-}$ mutant P14 oocytes when tested by RT-qPCR (Fig. 3e, Supplementary Fig. 2i). Thus, in P14 oocytes TBPL2 is regulating the transcription of many genes coding for factors, which are in turn crucial in regulating the stability and translation of the mRNA stock deposited during early oogenesis, as well as transcription of meiosis II- and cell cycle-related genes to prepare the growing oocytes for the upcoming meiotic cell division.

A remarkable feature of oocyte is the very high expression of retrotransposons driven by Pol II transcription (see Introduction). As expected, in WT P7 and P14 oocytes the expression of ERVs was found to be the most abundant[27,42] (Supplementary Fig. 3a-c). Importantly, the transcription of the vast majority of MaLR elements was the most affected in *Tbpl2*$^{-/-}$ mutant oocytes at P7 and P14 (Fig. 4). Among them, three highly expressed members, *MT-int*, *MTA_Mm*, and *MTA_Mm-int*, were dramatically down-regulated in P7 and P14 *Tbpl2*$^{-/-}$ mutant oocytes (Supplementary Fig. 3d, e). As in P14 oocytes TBPL2 depletion is reducing transcription more than 4-fold from MaLR ERVs, which often serve as promoters for neighbouring genes[27,42], TBPL2 could seriously deregulate oocyte-specific transcription and consequent genome activation.

Therefore, this is the first demonstration that TBPL2 is orchestrating the *de novo* restructuration of the maternal transcriptome and that TBPL2 is crucial for indirectly silencing the translation of the earlier deposited TBP-dependent transcripts.

TBPL2-driven promoters contain TATA box and are sharp

The promoter usage changes during zebrafish maternal to zygotic transition revealed different rules of transcriptional initiation in oocyte and in embryo, driven by independent and often overlapping sets of promoter "codes" [23]. Importantly, this switch has not yet been demonstrated in mammals and the role of TBPL2 in this switch during oogenesis remained to be investigated. To this end, we mapped the TSS usage by carrying out super-low input carrier-CAGE (SLIC-CAGE) [43] from WT and *Tbpl2*$^{-/-}$ P14 oocytes. To characterize only the TBPL2-driven promoters, we removed the CAGE tags present in the *Tbpl2*$^{-/-}$ dataset from the WT P14 dataset, to eliminate transcripts that have been deposited at earlier stages (hereafter called "TBPL2-dependent"). Conversely, the *Tbpl2*$^{-/-}$ dataset corresponds to the TBP/TFIID-dependent, or TBPL2-independent TSSs (hereafter called "TBPL2-independent").

Next, we analysed the genome-wide enrichment of T- and/or A-rich (WW) dinucleotide motifs within the -250/+250 region centred on the dominant TSSs of the TBPL2-specific-only and TBPL2-independent-only oocyte TSS clusters (Fig. 5a, b). TBPL2-dependent TSS clusters are strongly enriched in a well-defined WW motif around their -30 bp region (Fig. 5a, red arrowhead) [44]. In contrast, only about 1/3rd of the TBPL2-independent TSS clusters contained WW-enriched motifs at a similar position (Fig. 5b, red arrowhead), as would be expected from promoters that lack maternal promoter code determinants[23,44]. As canonical TATA boxes are often associated with tissue-specific gene promoters, we investigated whether the above observed WW motif densities correspond to TATA boxes using the TBP position weight matrix (PWM) from the JASPAR database as a reference. To this end the presence of TATA boxes was analysed in the TSS clusters of the two data sets and revealed that TBPL2-dependent TSS clusters were enriched in high quality TATA boxes, including a clear increase in the proportion of canonical TATA boxes, when compared to TBPL2-independent TSS clusters (Fig. 5c). Genome browser view snapshots indicate that TSS clusters in P14 WT oocytes tend to be sharp and are associated with TATA-like motifs

277 (Supplementary Fig. 4a, b). Analysis of the global distribution of the number of TSSs and of
278 the width of the TSS clusters in the above defined two categories confirmed that TBPL2-
279 dependent TSS are sharper compared to the TBPL2-independent TSS clusters (Supplementary
280 Fig. 4c, d).

281 In order to test whether TBPL2 controls transcription initiation from maternal promoter
282 code determinants, we grouped the expression profiles corresponding to each consensus TSS
283 clusters, to characterise promoter activity profiles among datasets by performing self-
284 organizing maps (SOM) [45] (Supplementary Fig. 4e). We then focussed on the two most
285 distinct SOM groups: the down-regulated promoters (blue group, containing 9442 consensus
286 TSS clusters) (Fig. 5d) and the up-regulated promoters (red group, with 6900 consensus TSS
287 clusters) (Fig. 5e). Motif analyses of these two categories of promoters in their -35/+5 regions
288 relative to the different dominant TSSs indicated that only the core promoters associated to
289 TBPL2-dependent dominant TSSs belonging to the down-regulated gene promoters contain a
290 well-defined 7 bp long TATA box-like motif (W-box) in their -31 to -24 regions (Fig. 5f, g,
291 Supplementary Fig. 4f-i). Importantly, W-box associated TSSs architecture usage distribution
292 for these TBPL2-dependent dominant TSSs was sharp (Supplementary Fig. 4j, l), as expected
293 for motif-dependent transcriptional initiation[23,44]. In contrast, TBPL2-independent TSSs
294 belonging to the up-regulated promoters exert a much broader TSS pattern (Supplementary
295 Fig. 4k, m). Interestingly, GO analyses of the genes associated with the down-regulated
296 promoters revealed a strong association with deadenylation/decapping/decay activity
297 (Supplementary Fig. 4n-p, Supplementary Data 7), further confirming our initial RNA-seq
298 analysis observations (Fig. 3).

299 Importantly, TSS architecture analyses of the TBPL2-dependent MaLR ERV TSSs
300 indicated that the majority of MaLR core promoters contain high quality TATA box motif
301 (median of the TATA box PWM match is 85%, Fig. 5h-j). These observations together

302 demonstrate that the TBPL2/TFIIA complex drives transcription initiation primarily from
303 core promoters that contain a TATA box-like motif in their core promoter and directs sharp
304 transcription initiation from the corresponding promoter regions to overhaul the growing
305 oocyte transcriptome.

306 In addition, we observed that TSS usage can shift within the promoter of individual
307 genes depending on the genetic background (Supplementary Fig. 4b). To get more insights in
308 these promoter architecture differences, we identified genome-wide 6429 shifting promoters
309 by comparing either TBPL2-dependent to TBPL2-independent TSS data. These results are
310 consistent with TSS shifts between somatic and maternal promoter codes occurring either in
311 5', or 3' directions (Fig. 6a, Supplementary Fig. 4q) [44]. WW motif analysis indicated that on
312 each shifting promoter, TBPL2-dependent dominant TSSs are associated with WW motifs,
313 while TBPL2-independent dominant TSSs are not (Fig. 6b). In addition, the TATA box PWM
314 match analyses indicated that these WW motifs are enriched in TATA box like elements
315 compared to the corresponding TBPL2-independent shifting TSSs (Fig. 6c). Thus, our
316 experiments provide a direct demonstration that TBP/TFIID and TBPL2/TFIIA machineries
317 recognize two distinct sequences co-existing in promoters of the same genes with TBPL2
318 directing a stronger WW/TATA box-dependent sharp TSS selection in them.

319

320

Discussion

In this study, we showed that a unique basal transcription machinery composed of TBPL2 associated with TFIIA is controlling transcription initiation during oocyte growth, orchestrating a transcriptome change prior to fertilization using an oocyte-specific TTS usage.

TBPL2 expression in mouse is limited to the oocytes and in its absence, oocytes fail to grow and *Tbpl2*$^{-/-}$ mouse females are sterile[16,28]. In a mirroring situation, TBPL1 (TRF2) expression is enriched during spermatogenesis and male germ cells lacking TBPL1 are blocked between the transition from late round spermatids to early elongating spermatids[14,15]. An interesting parallel between TBPL2 and TBPL1 is that both TBP-type factors form endogenous stable complexes with TFIIA. The beginning of TBPL2 accumulation in the oocyte nuclei, or TRF2 accumulation in male germ cell nuclei coincides with the phase of meiosis I[15,28,46]. It is thus conceivable that TBPL2-TFIIA in oocytes, or TRF2-TFIIA during spermatogenesis are involved in the control of gene expression in a meiotic context to set up the corresponding transcriptome. Interestingly, both transcription complexes seem to function in a compacted chromatin environment in which TBP/TFIID probably cannot. However, while TBPL2 and TBP show contrasting expression patterns in the oocytes[28], TBPL1 and TBP are co-expressed in spermatids[46,47] and it has been suggested that TBPL1 is a testis-specific subunit of TFIIA that is recruited to PIC containing TFIID and might not primarily act independently of TFIID/TBP to control gene expression in round spermatids[48]. While TBPL1 forms a complex also with the TFIIA-αβ paralogue, ALF, in testis[48-50], TBPL2 does not stably associate with ALF, in spite of the fact that it is expressed in oocytes[50].

TBP-like factors are bipartite proteins with variable N-terminal domains and a relatively well conserved shared C-terminal domains (core domains) forming a saddle-like structure with a concave surface that is known to bind to DNA[17]. Interestingly, TBPL1 has a very short N-terminal domain[5,18] suggesting that it lost some abilities to interact with partners.

346 Our data suggest that despite their very high similarity (92% identity between the core
347 domains of TBP and TBPL2 (reviewed in [51]), TBP and TBPL2 display different properties as
348 they seem to recognize different DNA sequences to regulate gene promoters with different
349 promoter architectures. Our IP-MS analyses from ovary WCE indicate that contrary to TBP,
350 TBPL2 does not interact with TAFs in growing oocytes. Our analyses in the NIH3T3-II10
351 cells that overexpresses TBPL2 showed that TBPL2 can interact with TAFs in this artificial
352 situation, albeit with less affinity compared to TFIIA, or TBP-TAFs interactions. Our
353 transcriptomic data indicates that all *Taf* mRNAs, except *Taf7l* are detected in growing
354 oocytes (Supplementary Data 5). However, whether they are also expressed in oocytes at the
355 protein level is not yet known, except for TAF4B that has been detected in female neonate
356 oocytes[52]. Nevertheless, our data suggest that TAF7 is expressed, but localized to the
357 cytoplasm. It could be conceivable that, similarly to *Tbp* mRNA that is transcribed, but not
358 translated in oocytes[53], *Taf* mRNA translations (other than *Taf7*) are also inhibited and as a
359 result the canonical TFIID, or its building blocks, cannot be assembled, and as a result the
360 canonical TFIID is not present in the nuclei of growing oocytes. Another reason why TBPL2
361 does not interact with TAFs, or ALF, but rather interacts with TFIIA could be its N-terminal
362 domain that is very different from TBP (only 23% identity[51]).

363 TBPL2 proteins from different vertebrates show a high degree of similarity in their C-
364 terminal core domains amongst themselves; but display very little conservation in their N-
365 terminal domains[12]. It is interesting to note that TBPL2 deficiency leads to an embryonic
366 phenotypes in Xenopus[13] and zebrafish[12], because, contrary to the mouse, TBPL2 is still
367 present in the embryo after fertilization and thus may act in parallel with TBP in the
368 transcription of specific embryonic genes[10,54]. The molecular mechanism by which TBPL2
369 controls the transcription of these specific sets of genes in frogs and in fish has not been

370 studied. In contrary, TBPL2 in mammals are only expressed in growing oocytes and the only
371 phenotype that can be observed in mammals is female sterility[16,29].

372 LTR retrotransposons, also known as ERVs, constitute ~10% of the mouse genome
373 (reviewed in [55]). While their expression is generally suppressed by DNA methylation and/or
374 repressive histone modifications, a subset of ERV subfamilies retain transcriptional activity in
375 specific cell types [56]. ERVs are especially active in germ cells and early embryos (reviewed in
376 [26]). Indeed, many genome-wide transcripts are initiated in LTRs, such as for example of
377 MaLRs in mouse oocytes, which constitute ~5% of the genome[57]. Members of the MT
378 subfamily of MaLRs are particularly active in oocytes and hundreds of MT LTRs have been
379 co-opted as oocyte-specific gene promoters[27,58]. As LTR-initiated transcription units shape
380 also the oocyte methylome, it will be important to analyse also how TBPL2 influences DNA
381 methylation in oocytes.

382 Oocytes display remarkable post-transcriptional regulatory mechanisms that control
383 mRNA stability and translation. During oogenesis, the oocyte genome is transcriptionally
384 active, and the newly synthesized maternal mRNAs are either translated or stored in a
385 dormant form (reviewed in [37]). The newly synthesized transcripts receive a long poly(A) tail
386 and subsequently undergo poly(A) shortening in the oocyte cytoplasm, preventing translation.
387 Until resumption of meiosis, mRNAs with a short poly(A) tail are stored in the cytoplasm in a
388 dormant form (for a review, see [59]). Thus, poly(A) tail deadenylation, amongst other
389 activities, coordinates post-transcriptional regulation of the oocyte mRNA pool. Interestingly,
390 TBPL2 is regulating the activity of several deadenylation/decapping/decay complexes and in
391 the absence of TBPL2, we observed apparent stabilization of a significant number of
392 transcripts, suggesting that in wild type oocytes TBPL2 is indirectly inhibiting the translation
393 of mRNAs, and/or inducing the degradation of the mRNAs, previously deposited by
394 TFIID/TBP in the primordial follicular oocytes (Fig. 7). To put in place the growing oocyte

395 specific maternal transcriptome TBPL2 is controlling the production of new mRNAs using a
396 maternal specific TSS grammar, as most of these transcripts will remain in the oocyte after
397 transcriptional quiescence. Remarkably, as TBPL2 does not interact with Pol I and Pol III
398 transcription machineries in the growing oocytes, this strongly suggest that rRNA and tRNA
399 are deposited very early during oogenesis in amounts sufficient for the initiation of
400 development.

401 Therefore, it seems that TBPL2 contributes to establish a novel TBPL2-dependent
402 growing oocyte transcriptome and consequent proteome required for further development and
403 oocyte competence for fertilization (Fig. 7). The indirect regulation of previously deposited
404 mRNAs by a global transcription regulator resembles the well characterised maternal to
405 zygotic transition (MZT), during which a clearance of inherited transcriptome is mediated by
406 *de novo* gene products generated by newly activated transcription machinery (reviewed in [59]).
407 At hundreds of gene promoters, two distinct TSS-defining "grammars" co-exist in close
408 proximity genome-wide and are differentially utilised in either TBPL2/TFIIA in
409 primary/secondary follicular oocytes, or by TBP/TFIID in primordial follicular oocytes or in
410 the fertilized embryo. This again shows a striking parallel to MZT[23], where multiple layers of
411 information are embedded in the same promoter sequence, each representing a different type
412 of regulatory grammar interpreted by dedicated transcription machinery depending on the
413 cellular environment.
414

Methods

Cell lines and cell culture

The NIH3T3-II10 line overexpressing TBPL2 and the control NIH3T3-K2 have already been described[28] and were maintained in high glucose DMEM supplemented with 10% of new-born calf serum at 37°C in 5% CO_2.

Whole cell extracts

NIH3T3-II10 and NIH3T3-K2 cells cultured in 15 cm dish were washed twice with 1x PBS, subsequently harvested by scrapping on ice. Harvested cells were centrifuged 1000 g at 4°C for 5 min and then resuspended in 1 packed cell volume of whole cell extraction buffer (20 mM Tris HCl pH7.5, 2 mM DTT, 20% Glycerol, 400 mM KCl, 1x Protease inhibitor cocktail (PIC, Roche)). Cell lysates were frozen in liquid nitrogen and thawed on ice for 3 times, followed by centrifugation at 20817 g, at 4°C for 15 min. The supernatant was collected and protein concentration was measured by Bradford protein assay (Bio-Rad). The cell extracts were used directly for immunoprecipitation and western blot, or stored at −80°C.

Ovaries collected from post-natal day 14 (P14) CD1 and C57BL/6N female mice were homogenized in whole cell extraction buffer [20 mM Tris HCl pH7.5, 2 mM DTT, 20% Glycerol, 400 mM KCl, 5x PIC (Roche)]. Cell lysates were frozen in liquid nitrogen and thawed on ice for 3 times, followed by centrifugation at 20817 g, at 4°C for 15 min. The supernatant extracts were used directly for immunoprecipitation.

Antibodies and antibody purification

The antibodies are listed in Supplementary Table 1. The IGBMC antibody facility raised the anti-TBPL2 polyclonal 3024 serum against the CPDEHGSELNLNSNSSPDPQ peptide

(amino acids 111-129) coupled to ovalbumin and injected into one 2 months-old female New-Zeland rabbit. The resulting serum was affinity purified by using the Sulfolink Coupling Gel (Pierce) following the manufacturer's recommendations.

Immunoprecipitation

Ovary extract were incubated with anti-GST (10 µg per IP), anti-TBP (10 µg per IP), anti-TBPL2 (3024, 12 µg (36 µg for gel filtration) per IP), anti-TAF7 (10 µg per IP) or anti-TAF10 (10 µg per IP) coated Dynabeads (Invitrogen) at 4°C overnight. After incubation, beads were washed 3 x 5min at 4°C with 500 mM KCl buffer [25 mM Tris-HCl (pH 7.9), 5 mM MgCl2, 10% glycerol, 0.1% NP40, 2 mM DTT, 500 mM KCl and 1x PIC (Roche)], then washed 3 x 5min at 4°C with 100 mM KCl buffer (25 mM Tris-HCl pH 7.9, 5 mM MgCl2, 10% glycerol, 0.1% NP40, 2 mM DTT, 100 mM KCl and 1x). Immunoprecipitated proteins were eluted with 0.1 M glycine pH 2.8 and neutralized with 1.5 M Tris-HCl pH 8.8.

Immunoprecipitation performed from whole cell extracts of NIH3T3-II10 and NIH3T3-K2 cells were following the same procedures with protein G Sepharose beads (GE Healthcare): 18 µg rabbit anti-TBPL2 (3024) and 15 µg anti-TBP per IP.

Western blot analyses

Protein samples (15-25 µg of cell extracts or 15 µL of IP elution) were mixed with 1/4th volume of loading buffer (100 mM Tris-HCl pH 6.8, 30% glycerol, 4% SDS, 0.2% bromophenol blue and freshly added 100 mM DTT) and boiled for 10 min. Samples were then resolved on a 10 % SDS-PAGE and transferred to nitrocellulose membrane (Protran, Amersham). Membranes were blocked in 3% non-fat milk in 1x PBS at room temperature (RT) for 30 min, and subsequently incubated with the primary antibody overnight at 4°C (dilution 1/1000). Membranes were washed three times (10 min each) with 1x PBS - 0.05%

Tween20. Membranes were then incubated with HRP-coupled goat anti Mouse Ig (Jackson ImmunoResearch, #115-036-071, dilution 1/10000) or HRP-coupled goat anti-Rabbit Ig (Jackson ImmunoResearch, #115-035-144, dilution 1/10000) for 1 hour at RT, followed by ECL detection (Thermo Fisher). The signal was acquired with the ChemiDoc imaging system (Bio-Rad).

Mass spectrometry analyzes and NSAF calculations

Samples were TCA precipitated, reduced, alkylated and digested with LysC and Trypsin at 37°C overnight. After C18 desalting, samples were analyzed using an Ultimate 3000 nano-RSLC (Thermo Scientific, San Jose, California) coupled in line with a linear trap Quadrupole (LTQ)-Orbitrap ELITE mass spectrometer via a nano-electrospray ionization source (Thermo Scientific). Peptide mixtures were loaded on a C18 Acclaim PepMap100 trap column (75 µm inner diameter × 2 cm, 3 µm, 100 Å; Thermo Fisher Scientific) for 3.5 min at 5 µL/min with 2% acetonitrile (ACN), 0.1% formic acid in H_2O and then separated on a C18 Accucore nano-column (75 µm inner diameter × 50 cm, 2.6 µm, 150 Å; Thermo Fisher Scientific) with a 240 minutes linear gradient from 5% to 50% buffer B (A: 0.1% FA in H_2O / B: 80% ACN, 0.08% FA in H_2O) followed with 10 min at 99% B. The total duration was set to 280 minutes at a flow rate of 200 nL/min.

Proteins were identified by database searching using SequestHT with Proteome Discoverer 1.4 software (Thermo Fisher Scientific) a combined Mus musculus database generated using Uniprot [https://www.uniprot.org/uniprot/?query=proteome:UP000000589&sort=score] (Swissprot, release 2015_11, 16730 entries) where 5 interesting proteins sequences (TrEMBL entries: TAF4, ATXN7L2, TADA2B, BTAF1 and SUPT3) were added. Precursor and fragment mass tolerances were set at 7 ppm and 0.5 Da respectively, and up to 2 missed cleavages were allowed. Oxidation (M) was set as variable modification, and

Carbamidomethylation© as fixed modification. Peptides were filtered with a false discovery rate (FDR) at 5 %, rank 1 and proteins were identified with 1 unique peptide. Normalized spectral abundance factor (NSAF)[31] were calculated using custom R scripts (R software version 3.5.3). Only proteins detected in at least 2 out of 3 of the technical or biological replicates were considered for further analyses.

Gel filtration

A Superose 6 (10/300) column was equilibrated with buffer consisting of 25mM Tris HCl pH 7.9, 5 mM MgCl2, 150 mM KCl, 5% Glycerol, 1 mM DTT and 1x PIC (Roche). Five hundred µL of whole cell extracts containing ~5 mg of protein were injected in an ÄKTA avant chromatography system (Cytiva) and run at 0.4 mL/min. Protein detection was performed by absorbance at 280 nm and 260 nm. Five hundred µL fractions were collected and analysed by Western blot and IP-MS.

Animal experimentation

Animal experimentations were carried out according to animal welfare regulations and guidelines of the French Ministry of Agriculture and procedures were approved by the French Ministry for Higher Education and Research ethical committee C2EA-17 (project n°2018031209153651). The Tg(*Zp3-Cre*), *Taf7*^{flox} and *Tbpl2*$^{-}$ mouse lines have already been described[16,33,60].

Histology analyses of ovaries

Ovaries were collected from 6 weeks-old Tg(*Zp3-Cre*/+);*Taf7*$^{flox/+}$ and Tg(*Zp3-Cre*/+);*Taf7*$^{flox/\Delta}$ oocyte specific mutant females, fixed in 4% paraformaldehyde (Electron Microscopy Sciences) over-night at 4°C, washed 3 times in PBS at room temperature and

embedded in paraffin. Five µm-thick sections were stained with haematoxylin and eosin and images were acquired using a slide scanner Nanozoomer 2.0HT (Hamamatsu Photonics).

Immunolocalization of TAF7 in the oocytes

Ovaries were dissected in PBS, fixed overnight in 4%PFA/PBS at 4°C, rinsed three times in PBS, equilibrated in 30% sucrose/PBS and embedded in Cryomatrix (Thermo Scientific) in liquid nitrogen vapor. Fifteen µm-thick sections were obtained on a Leica cryostat and stored at -80°C. Sections were rehydrated in TBS (50 mM Tris, 150 mM NaCl, pH7.5), and permeabilized with 0.5% Triton-X-100 (Sigma) and rinsed twice again in TBS before blocking in 3% BSA, 1% Goat serum, 0.1% Tween-20 (Sigma). Immunolabeling was then performed using M.O.M® Immunodetection Kit, Basic (Vector Laboratories, BMK-2202). Purified anti-TAF7 rabbit polyclonal antibody (dilution 1/300) was revealed using an Alexa Fluor 488 goat anti-rabbit IgG (Invitrogen #A-11108, dilution 1/1000). Sections were counterstained with DAPI (4′,6-diamidino-2-phenylindole dihydrochloride; Molecular Probes). Pictures were taken using a TCS SP5 Inverted confocal (Leica) with a 40x Plan APO objective (CX PL APO 40x/1.25-0.75 OIL CS) and analyzed using Fiji 2.0.

Supervovulation

Five units of pregnant mare serum (PMS) was injected intraperitoneally in 4-week-old female mice between 2-4 pm. After 44-46 hours, GV oocytes were collected from the ovaries by puncturing with needles.

Oocytes collection

After dissection, ovaries are freed from adhering tissues in 1x PBS. Series of 6 ovaries were digested in 500 µL of 2 mg/mL Collagenase (SIGMA), 0.025% Trypsin (SIGMA) and 0.5

mg/mL type IV-S hyaluronidase (SIGMA), on a ThermoMixer (Eppendorf) with gentle agitation for 20 minutes. The digestion was then stopped by the addition of 1 mL of 37°C pre-warmed αMEM - 5% FBS. The oocytes were then size-selected under a binocular.

RNA preparation

Pool of 100-200 oocytes collected were washed through several M2 drops, and total RNA was isolated using NucleoSpin RNAXS kit (Macherey-Nagel) according to the user manual. RNA quality and quantity were evaluated using a Bioanalyzer. Between 5-10 ng of RNA was obtained from each pool of oocytes.

RNA-seq analyses

PolyA+ RNA seq libraries were prepared using the SMART-Seq v4 UltraLow Input RNA kit (Clonetch) followed by the Nextera XT DNA library Prep kit (Illumina) according to the manufacturer recommendations from 3 biological replicates for each condition (P7 wild-type (WT), P7 *Tbpl2*$^{-/-}$ mutant, P14 WT and P14 *Tbpl2*$^{-/-}$ mutant oocytes) and sequenced 50 pb single end using an Illumina HiSeq 4000 (GenomEast platform, IGBMC).

Reads were preprocessed in order to remove adapter, polyA and low-quality sequences (Phred quality score below 20). After this preprocessing, reads shorter than 40 bases were discarded for further analysis. These preprocessing steps were performed using cutadapt version 1.10[61]. Reads were mapped to spike sequences using bowtie version 2.2.8[62], and reads mapping to spike sequences were removed for further analysis. Reads were then mapped onto the mm10 assembly of *Mus musculus* genome using STAR version 2.7.0f[63]. Gene expression quantification was performed from uniquely aligned reads using htseq-count version 0.9.1[64], with annotations from Ensembl version 96 and “union" mode. Read counts were normalized across samples with the median-of-ratios method, to make these counts comparable between

samples and differential gene analysis were performed using the DESeq2 version 1.22.2[65]. All the figures were generated using R software version 3.5.3.

RT-qPCR

Complementary DNA was prepared using random hexamer oligonucleotides and SuperScript IV Reverse Transcriptase (Invitrogen) and amplified using LightCycler® 480 SYBR Green I Master (Roche) on a LightCycler® 480 II (Roche). Primers used for qPCR analysis are listed in Supplementary Table 2.

Repeat element analyses

Data were processed as already described[66] using Bowtie1 (version 1.2.2) [67] instead of Maq. The repeatMasker annotation was used to identified the different types of repeat elements (Smit, AFA, Hubley, R & Green, P. RepeatMasker Open-4.0. 2013-2015 http://www.repeatmasker.org). Differential expression analyses were performed using DESeq2 (version 1.22.2) [65]. All the figures were generated using R custom scripts (version 3.5.3).

SLIC-CAGE analyses

Twenty-eight and 13 ng of total RNA isolated from P14 oocytes (biological replicate 1 and replicate 2, approximately 500-1000 oocytes pooled for each replicate) and 15 ng of total RNA isolated from P14 *Tbpl2*$^{-/-}$ mutant oocytes (approximately 550 pooled oocytes) were used for SLIC-CAGE TSS mapping[43]. Briefly, 5 µg of the carrier RNA mix were added to each sample prior to reverse transcription, followed by the cap-trapping steps designed to isolate capped RNA polymerase II transcripts. The carrier was degraded from the final library prior to sequencing using homing endonucleases. The target library derived from the oocyte

RNA polymerase II transcripts was PCR-amplified (15 cycles for P14 WT, 16 cycles for P14 *Tbpl2*$^{-/-}$ mutant) and purified using AMPure beads (Beckman Coulter) to remove short PCR artifacts (< 200bp, size selection using 0.8 x AMPure beads to sample ratio). The libraries were sequenced using HiSeq2500 Illumina platform in single-end, 50 bp mode (Genomics Facility, MRC, LMS).

Sequenced SLIC-CAGE reads were mapped to the reference *M. musculus* genome (mm10 assembly) using the Bowtie2[62] with parameters that allow zero mismatches per seed sequence (22 nucleotides). Uniquely mapped reads were kept for downstream analyses using CAGEr Bioconductor package (version 1.20.0) [68] and custom R/Bioconductor scripts. Bam files were imported into R using the CAGEr package, where the mismatching additional G, if added through the template-free activity of the reverse transcriptase, was removed. Same samples sequenced on different lanes and biological replicates were merged prior to final analyses.

Promoter analyses

In order to consider only the CAGE TSS dependent only on TBPL2, we removed all the P14 WT CAGE tags at position where CAGE tags were also present in the P14 *Tbpl2*$^{-/-}$ mutant CAGE tags dataset: for the rest of the analysis, this dataset was called “TBPL2-dependent” and we compared it to the P14 *Tbpl2*$^{-/-}$ mutant CAGE data (hereafter called “TBPL2-independent”). Briefly, a CAGE set object was created from the TBPL2-dependent and TBPL2-independent CTSS files using CAGEr Bioconductor package (version 1.20.0) [68], data were normalized using normalizeTagCount (fitInRange = c(5,1000), alpha = 1.53, T = 1e6) and the powerLaw option. Cluster of CTSS were collected using clusterCTSS (threshold = 1, thresholdIsTpm = TRUE, nrPassThreshold = 1, method = "distclu", maxDist = 20, removeSingletons = TRUE, keepSingletonsAbove = 5). Width of the TSS regions was calculated using cumulativeCTSSdistribution and quantilePositions (clusters = "tagClusters",

615 qLow = 0.1, qUp = 0.9): interquantile width corresponds to the 10th-90th percentile of the total
616 tag cluster signal. In order to compare the different samples, consensus promoters were
617 computed using aggregateTagCluster (tpmThreshold = 3, qLow = 0.1, qUp = 0.9, maxDist =
618 100). Self-organizing map (SOM) expression profiling was performed using
619 getExpressionProfiles using a tpmThrshold of 3, the method "som", xDim = 3 and yDim = 2.
620 Shifting TSS were obtained after calculation of the cumulative distribution along the
621 consensus clusters using cumulativeCTSSdistribution and calculation of the shift score using
622 scoreShift with the Kolomogorov-Smirnov test. Shifting promoters were extracted using
623 getShiftingPromoters (tpmThreshold = 3, scoreThreshold = -Inf, fdrThreshold = 0.01).
624 TSSs corresponding to the MaLR-ERVS were identified after annotation using HOMER
625 (version 4.10) [69].
626 Sequences analyses were performed using Bioconductor R seqPattern (version 1.14) and R
627 custom scripts. WW dinucleotides enrichment was computed using plotPatternDensityMap on
628 -250/+250 regions centered on the dominant TSSs. TATA box position weight matrix (PWM)
629 matches analyses was performed using the MotifScanScores function applied on the -35/-20
630 sequences centered on the dominant TSSs, using the TBP PWM provided in the SeqPattern
631 package (derived from the JASPAR data base). Distribution of the best match for each
632 sequence was then plotted. Sequence Logo were created using Bioconductor R package
633 SeqLogo.
634

Data availability

The datasets generated during the current study are available in different repositories: proteomic data; ProteomeXchange PRIDE database (PXD0316347 [http://www.ebi.ac.uk/pride/archive/projects/PXD016347]), RNA-seq data; Gene Expression Omnibus database (GSE140090 [https://www.ncbi.nlm.nih.gov/geo/query/acc.cgi?acc=GSE140090]") and SLIC-CAGE data; ArrayExpress (E-MTAB-8866 [https://www.ebi.ac.uk/arrayexpress/experiments/E-MTAB-8866/]).

Code availability

RNA-seq data was analysed using Bioconductor package DESeq2, SLIC-CAGE data was analysed using Bioconductor package CAGEr. All custom code is available upon request.

References

1. Roeder, R. G. 50+ years of eukaryotic transcription: an expanding universe of factors and mechanisms. *Nat Struct Mol Biol* **26,** 783–791 (2019).
2. Haberle, V. & Stark, A. Eukaryotic core promoters and the functional basis of transcription initiation. *Nat Rev Mol Cell Biol* **19,** 621–637 (2018).
3. Tora, L. A unified nomenclature for TATA box binding protein (TBP)-associated factors (TAFs) involved in RNA polymerase II transcription. *Genes Dev* **16,** 673–675 (2002).
4. Levine, M., Cattoglio, C. & Tjian, R. Looping back to leap forward: transcription enters a new era. *Cell* **157,** 13–25 (2014).
5. Ohbayashi, T., Makino, Y. & Tamura, T. A. Identification of a mouse TBP-like protein (TLP) distantly related to the drosophila TBP-related factor. *Nucleic Acids Res* **27,** 750–755 (1999).
6. Teichmann, M. *et al.* Human TATA-binding protein-related factor-2 (hTRF2) stably associates with hTFIIA in HeLa cells. *Proceedings of the National Academy of Sciences* **96,** 13720–13725 (1999).
7. Dantonel, J. C., Quintin, S., Lakatos, L., Labouesse, M. & Tora, L. TBP-like factor is required for embryonic RNA polymerase II transcription in C. elegans. *Mol Cell* **6,** 715–722 (2000).
8. Kaltenbach, L., Horner, M. A., Rothman, J. H. & Mango, S. E. The TBP-like factor CeTLF is required to activate RNA polymerase II transcription during C. elegans embryogenesis. *Mol Cell* **6,** 705–713 (2000).
9. Veenstra, G. J. C. Distinct Roles for TBP and TBP-Like Factor in Early Embryonic Gene Transcription in Xenopus. *Science* **290,** 2312–2315 (2000).
10. Müller, F., Lakatos, L., Dantonel, J., Strähle, U. & Tora, L. TBP is not universally required for zygotic RNA polymerase II transcription in zebrafish. *Curr Biol* **11,** 282–287 (2001).
11. Persengiev, S. P. *et al.* TRF3, a TATA-box-binding protein-related factor, is vertebrate-specific and widely expressed. *Proceedings of the National Academy of Sciences* **100,** 14887–14891 (2003).
12. Bártfai, R. *et al.* TBP2, a vertebrate-specific member of the TBP family, is required in embryonic development of zebrafish. *Curr Biol* **14,** 593–598 (2004).
13. Jallow, Z., Jacobi, U. G., Weeks, D. L., Dawid, I. B. & Veenstra, G. J. C. Specialized and redundant roles of TBP and a vertebrate-specific TBP paralog in embryonic gene regulation in Xenopus. *Proceedings of the National Academy of Sciences* **101,** 13525–13530 (2004).
14. Zhang, D., Penttila, T. L., Morris, P. L., Teichmann, M. & Roeder, R. G. Spermiogenesis deficiency in mice lacking the Trf2 gene. *Science* **292,** 1153–1155 (2001).
15. Martianov, I. *et al.* Late arrest of spermiogenesis and germ cell apoptosis in mice lacking the TBP-like TLF/TRF2 gene. *Mol Cell* **7,** 509–515 (2001).
16. Gazdag, E. *et al.* TBP2 is essential for germ cell development by regulating transcription and chromatin condensation in the oocyte. *Genes Dev* **23,** 2210–2223 (2009).
17. Hernandez, N. TBP, a universal eukaryotic transcription factor? *Genes Dev* **7,** 1291–1308 (1993).
18. Rabenstein, M. D., Zhou, S., Lis, J. T. & Tjian, R. TATA box-binding protein (TBP)-related factor 2 (TRF2), a third member of the TBP family. *Proceedings of the National Academy of Sciences* **96,** 4791–4796 (1999).

19. Hansen, S. K., Takada, S., Jacobson, R. H., Lis, J. T. & Tjian, R. Transcription properties of a cell type-specific TATA-binding protein, TRF. *Cell* **91,** 71–83 (1997).
20. Ohbayashi, T. *et al.* Vertebrate TBP-like protein (TLP/TRF2/TLF) stimulates TATA-less terminal deoxynucleotidyl transferase promoters in a transient reporter assay, and TFIIA-binding capacity of TLP is required for this function. *Nucleic Acids Res* **31,** 2127–2133 (2003).
21. Carninci, P. *et al.* Genome-wide analysis of mammalian promoter architecture and evolution. *Nat Genet* **38,** 626–635 (2006).
22. Lenhard, B., Sandelin, A. & Carninci, P. Metazoan promoters: emerging characteristics and insights into transcriptional regulation. *Nat Rev Genet* **13,** 233–245 (2012).
23. Haberle, V. *et al.* Two independent transcription initiation codes overlap on vertebrate core promoters. *Nature* **507,** 381–385 (2014).
24. Jagarlamudi, K. & Rajkovic, A. Oogenesis: Transcriptional regulators and mouse models. *Mol Cell Endocrinol* **356,** 31–39 (2012).
25. Pedersen, T. & Peters, H. Proposal for a classification of oocytes and follicles in the mouse ovary. *J. Reprod. Fertil.* **17,** 555–557 (1968).
26. Thompson, P. J., Macfarlan, T. S. & Lorincz, M. C. Long Terminal Repeats: From Parasitic Elements to Building Blocks of the Transcriptional Regulatory Repertoire. *Mol Cell* **62,** 766–776 (2016).
27. Peaston, A. E. *et al.* Retrotransposons regulate host genes in mouse oocytes and preimplantation embryos. *Dev Cell* **7,** 597–606 (2004).
28. Gazdag, E., Rajkovic, A., Torres-Padilla, M.-E. & Tora, L. Analysis of TATA-binding protein 2 (TBP2) and TBP expression suggests different roles for the two proteins in regulation of gene expression during oogenesis and early mouse development. *Reproduction* **134,** 51–62 (2007).
29. Malecova, B. *et al.* TBP/TFIID-dependent activation of MyoD target genes in skeletal muscle cells. *Elife* **5,** 23 (2016).
30. Deato, M. D. E. *et al.* MyoD targets TAF3/TRF3 to activate myogenin transcription. *Mol Cell* **32,** 96–105 (2008).
31. Zybailov, B. *et al.* Statistical analysis of membrane proteome expression changes in Saccharomyces cerevisiae. *J. Proteome Res.* **5,** 2339–2347 (2006).
32. Helmlinger, D. & Tora, L. Sharing the SAGA. *Trends Biochem. Sci.* **42,** 850–861 (2017).
33. Lewandoski, M., Wassarman, K. M. & Martin, G. R. Zp3–cre, a transgenic mouse line for the activation or inactivation of loxP-flanked target genes specifically in the female germ line. *Current Biology* **7,** 148–151 (1997).
34. Vannini, A. & Cramer, P. Conservation between the RNA polymerase I, II, and III transcription initiation machineries. *Mol Cell* **45,** 439–446 (2012).
35. Dong, J. *et al.* Growth differentiation factor-9 is required during early ovarian folliculogenesis. *Nature* **383,** 531–535 (1996).
36. Galloway, S. M. *et al.* Mutations in an oocyte-derived growth factor gene (BMP15) cause increased ovulation rate and infertility in a dosage-sensitive manner. *Nat Genet* **25,** 279–283 (2000).
37. Bettegowda, A. Mechanisms of maternal mRNA regulation: implications for mammalian early embryonic development. *Frontiers in Bioscience* **12,** 3713 (2007).
38. Timmers, H. T. M. & Tora, L. Transcript Buffering: A Balancing Act between mRNA Synthesis and mRNA Degradation. *Mol Cell* **72,** 10–17 (2018).
39. Yu, C. *et al.* BTG4 is a meiotic cell cycle-coupled maternal-zygotic-transition licensing factor in oocytes. *Nat Struct Mol Biol* **23,** 387–394 (2016).

40. Wolf, J. & Passmore, L. A. mRNA deadenylation by Pan2-Pan3. *Biochem. Soc. Trans.* **42,** 184–187 (2014).
41. Ma, J., Flemr, M., Strnad, H., Svoboda, P. & Schultz, R. M. Maternally recruited DCP1A and DCP2 contribute to messenger RNA degradation during oocyte maturation and genome activation in mouse. *Biol Reprod* **88,** 11 (2013).
42. Veselovska, L. *et al.* Deep sequencing and de novo assembly of the mouse oocyte transcriptome define the contribution of transcription to the DNA methylation landscape. *Genome Biol.* **16,** 209 (2015).
43. Cvetesic, N. *et al.* SLIC-CAGE: high-resolution transcription start site mapping using nanogram-levels of total RNA. *Genome Res.* **28,** 1943–1956 (2018).
44. Cvetesic, N. *et al.* Global regulatory transitions at core promoters demarcate the mammalian germline cycle. *bioRxiv* **11,** 2020.10.30.361865 (2020).
45. Törönen, P., Kolehmainen, M., Wong, G. & Castrén, E. Analysis of gene expression data using self-organizing maps. *FEBS Letters* **451,** 142–146 (1999).
46. Zhang, D., Penttila, T. L., Morris, P. L. & Roeder, R. G. Cell- and stage-specific high-level expression of TBP-related factor 2 (TRF2) during mouse spermatogenesis. *Mech Dev* **106,** 203–205 (2001).
47. Martianov, I. *et al.* Distinct functions of TBP and TLF/TRF2 during spermatogenesis: requirement of TLF for heterochromatic chromocenter formation in haploid round spermatids. *Development* **129,** 945–955 (2002).
48. Martianov, I., Velt, A., Davidson, G., Choukrallah, M.-A. & Davidson, I. TRF2 is recruited to the pre-initiation complex as a testis-specific subunit of TFIIA/ALF to promote haploid cell gene expression. *Sci Rep* **6,** 32069 (2016).
49. Upadhyaya, A. B., Lee, S. H. & DeJong, J. Identification of a general transcription factor TFIIAalpha/beta homolog selectively expressed in testis. *J Biol Chem* **274,** 18040–18048 (1999).
50. Xiao, L., Kim, M. & DeJong, J. Developmental and cell type-specific regulation of core promoter transcription factors in germ cells of frogs and mice. *Gene Expression Patterns* **6,** 409–419 (2006).
51. Müller, F., Zaucker, A. & Tora, L. Developmental regulation of transcription initiation: more than just changing the actors. *Curr Opin Genet Dev* **20,** 533–540 (2010).
52. Falender, A. E., Shimada, M., Lo, Y. K. & Richards, J. S. TAF4b, a TBP associated factor, is required for oocyte development and function. *Developmental Biology* **288,** 405–419 (2005).
53. Akhtar, W. & Veenstra, G. J. C. TBP2 is a substitute for TBP in Xenopus oocyte transcription. *BMC Biol.* **7,** 45 (2009).
54. Jacobi, U. G. *et al.* TBP paralogs accommodate metazoan- and vertebrate-specific developmental gene regulation. *EMBO J* **26,** 3900–3909 (2007).
55. Crichton, J. H., Dunican, D. S., Maclennan, M., Meehan, R. R. & Adams, I. R. Defending the genome from the enemy within: mechanisms of retrotransposon suppression in the mouse germline. *Cell Mol Life Sci* **71,** 1581–1605 (2014).
56. Faulkner, G. J. *et al.* The regulated retrotransposon transcriptome of mammalian cells. *Nat Genet* **41,** 563–571 (2009).
57. McCarthy, E. M. & McDonald, J. F. Long terminal repeat retrotransposons of Mus musculus. *Genome Biol.* **5,** R14 (2004).
58. Franke, V. *et al.* Long terminal repeats power evolution of genes and gene expression programs in mammalian oocytes and zygotes. *Genome Res.* **27,** 1384–1394 (2017).
59. Vastenhouw, N. L., Cao, W. X. & Lipshitz, H. D. The maternal-to-zygotic transition revisited. *Development* **146,** dev161471 (2019).

60. Gegonne, A. *et al.* The general transcription factor TAF7 is essential for embryonic development but not essential for the survival or differentiation of mature T cells. *Mol Cell Biol* **32,** 1984–1997 (2012).
61. Martin, M. Cutadapt removes adapter sequences from high-throughput sequencing reads. *EMBnet.journal* **17,** 10–12 (2011).
62. Langmead, B. & Salzberg, S. L. Fast gapped-read alignment with Bowtie 2. *Nat. Methods* **9,** 357–359 (2012).
63. Dobin, A. *et al.* STAR: ultrafast universal RNA-seq aligner. *Bioinformatics* **29,** 15–21 (2012).
64. Anders, S., Pyl, P. T. & Huber, W. HTSeq--a Python framework to work with high-throughput sequencing data. *Bioinformatics* **31,** 166–169 (2015).
65. Love, M. I., Huber, W. & Anders, S. Moderated estimation of fold change and dispersion for RNA-seq data with DESeq2. *Genome Biol.* **15,** 31 (2014).
66. Fadloun, A. *et al.* Chromatin signatures and retrotransposon profiling in mouse embryos reveal regulation of LINE-1 by RNA. *Nat Struct Mol Biol* **20,** 332–338 (2013).
67. Langmead, B., Trapnell, C., Pop, M. & Salzberg, S. L. Ultrafast and memory-efficient alignment of short DNA sequences to the human genome. *Genome Biol.* **10,** R25 (2009).
68. Haberle, V., Forrest, A. R. R., Hayashizaki, Y., Carninci, P. & Lenhard, B. CAGEr: precise TSS data retrieval and high-resolution promoterome mining for integrative analyses. *Nucleic Acids Res* **43,** e51–e51 (2015).
69. Heinz, S. *et al.* Simple combinations of lineage-determining transcription factors prime cis-regulatory elements required for macrophage and B cell identities. *Mol Cell* **38,** 576–589 (2010).

Acknowledgements

We thank D. Singer and A. Gegonne for the gift of the *Taf7*^{flox} mouse line and H. Stunnenberg for TFIIA antibodies. We would also like to thank D. Devys for critically reading the manuscript, all members of the Tora lab for thoughtful discussions and suggestions throughout the course of the work. We are grateful to I. Kukhtevich, M. Borsos, M.E. Torres Padilla, T. Gupta, L. Casini, G. Barzaghi and A. Krebs for help in preliminary experiments. We thank C. Hérouard and M. Jung from the GenomEAST platform for library preparation and preliminary analyses, P. Eberling for peptide synthesis, F. Ruffenach for proteomic analyses, G. Duval for polyclonal antibody generation, the histology platform, the IGBMC cell culture facility and S. Falcone, M. Poirot and F. Memedov of the IGBMC animal facility for animal care taking. This work was supported by funds from CNRS, INSERM, and Strasbourg University. This study was also supported by the European Research Council (ERC) Advanced grant (ERC-2013-340551, Birtoaction) and grant ANR-10-LABX-0030-INRT (to LT) and a French State fund managed by the Agence Nationale de la Recherche under the frame program Investissements d'Avenir ANR-10-IDEX-0002-02. IB and FM acknowledge support by Wellcome Trust Senior Investigator awards (106115/Z/14/Z and 106955/Z/15/Z, respectively).

Authors' contribution

CY, SDV and LT designed the study; SDV and LT supervised the project; CY performed all molecular lab and mouse experiments, VH performed immunolocalizations and helped for the histological analysis of ovaries, EG generated the anti-TBPL2 polyclonal antibodies, LN carried out the proteomic analyses, KG and IB carried out preliminary analyses, PH organized the SLIC-CAGE, NC carried out SLIC-CAGE analyses, NC and BL analysed the SLIC-CAGE data, and SDV analysed the proteomic, RNA-seq and SLIC-CAGE data. FM oriented the promoter analyses.

CY, FM, SDV and LT wrote the manuscript with contributions to manuscript text and figure legends from all authors. All authors gave final approval for publication.

Competing interests

The authors declare that they have no competing interests.

Additional Information

Supplementary information is available for this paper.

Correspondence and request for materials should be addressed to S. D. Vincent (vincent@igbmc.fr) or L. Tora (laszlo@igbmc.fr).

Figure legends

Fig. 1 TBPL2 does not assemble in a TFIID-like complex in growing oocytes. **a** Anti-TBPL2 immunoprecipitation followed by mass spectrometry (IP-MS) analysis from three biological replicates of mouse ovarian whole cell extracts (WCE). The color code for the different proteins or complexes is indicated on the right. NSAF; normalized spectral abundance factor. **b** Anti-TBP IP-MS from ovarian WCE (three technical triplicates). The color code is the same as in (**a**). **c-f** Sequential IP-MS experiment from ovarian WCE (three technical triplicates). Strategy of the sequential immunoprecipitation (**c**), anti-TAF7 IP-MS (**d**), followed by an anti-TAF10 IP-MS (**e**) and then an anti-TBPL2 IP-MS (**f**). The color code is the same as in (**a**). **g, h** Representative views of haematoxylin and eosin stained ovaries section from control (**e**) and oocyte-specific *Taf7* mutant (Tg(*Zp3-Cre*/+);*Taf7*$^{flox/\Delta}$, **f**) ovaries (analyses of 3 sections from 3 biological replicates). The presence of antral follicles is indicated by an asterisk. Scale bars: 500 µm. Grey dots indicate replicates and error bars, +/- standard error of the mean in (**a**, **b**, **d-f**).

Fig. 2 TBPL2 assembles into a TBPL2/TFIIA and TFIID-like complexes in NIH3T3 cells over-expressing TBPL2. **a** Anti-TBPL2 immunoprecipitation followed by mass spectrometry (IP-MS) analysis (three technical replicates) of NIH3T3 over-expressing TBPL2 (NIH3T3-II10) whole cell extracts (WCE). The color code for the different proteins or complexes is indicated on the right. **b** Anti-TBP IP-MS analysis (three technical replicates) of NIH3T3-II10 WCE. Color legend for the different proteins is the same as in (**a**). **c** Western blot of a Superose 6 gel filtration analysis of NIH3T3-II10 WCE probed with anti-TAF6 (top panel), anti-TBPL2 and anti-TFIIA-α (middle panels), and anti-TBP (bottom panel) antibodies. Fraction numbers are shown above each lane and the elution of known molecular mass

markers is indicated above the panels. The pooled fractions used for mass spectrometry analysis are indicated in red. **d** Anti-TBPL2 IP-MS analysis (three technical replicates) of the gel filtration fraction indicated in (**c**). The color code for the different proteins or complexes is indicated on the right. NSAF; normalized spectral abundance factor. **e** Schematic representation of the fundamental differences existing between TBPL2- and TBP-containing complexes in growing oocytes and NIH3T3-II10 cells. Grey dots indicate replicates and error bars, +/- standard error of the mean in (**a**, **b**, **d**).

Fig. 3 Expression of genes related to the mRNA deadenylation/decapping/decay pathways in growing *Tbpl2*$^{-/-}$ mutant oocytes. **a, b** Normalized Integrative Genomic Viewer (IGV) snapshots of *Bmp15* (**a**) and *Gdf9* (**b**) loci. Exons and introns are indicated. **c** Expression comparison between wild-type (WT) and *Tbpl2*$^{-/-}$ mutant post-natal day 14 (P14) oocytes (biological triplicates). Expression was normalized to the median size of the transcripts in kb. Grey dots correspond to non-significant genes and genes with high Cook's distance, light-blue dots to significant genes for an adjusted p value ≤ 0.05 and dark-blue dots to significant genes for an adjusted p value ≤ 0.05 and an absolute log2 fold change > 1, after two-sided Wald test and Benjamini-Hochberg correction for multiple comparison. The number of up- or down-regulated genes is indicated on the graph. **d** Down-regulated genes GO category analyses for the molecular functions (MF). The top ten most enriched significant GO categories for a FDR ≤ 0.05 are represented. **e** Heatmap of selected genes involved in mRNA decay, decapping or deadenylation pathways. Expression levels in fold-change (compared to the mean of WT) of three biological replicates of P14 WT and P14 *Tbpl2*$^{-/-}$ mutant oocytes are indicated. The fold change color legend is indicated at the bottom. The first column on the left corresponds to the log10 of expression, scale on the left.

907 **Fig. 4** Expression of the mammalian apparent LTR retrotransposons (MaLR) endogenous
908 retroviral elements (ERV) are down regulated in growing *Tbpl2*$^{-/-}$ mutant oocytes. **a-h**
909 Differential expression between wild type and *Tbpl2*$^{-/-}$ mutant post-natal day (P) 7 (**a-d**) and
910 P14 (**e-h**) oocytes of the different transposon classes; RNA transposon classes [LINEs (**a**, **e**),
911 SINEs (**b**, **f**) and ERVs (**c**, **g**)] and DNA transposons (DNAs (**d**, **h**)). The ERV sub-class III
912 mammalian apparent LTR retrotransposon (MaLR) family is the most severely affected in
913 *Tbpl2*$^{-/-}$ mutant oocytes at P7 and P14. Dot size and color are explained on the right side,
914 adjusted *p* value after two-sided Wald test and Benjamini-Hochberg correction for multiple
915 comparison.
916
917 **Fig. 5** Core promoter regions of TBPL2 specific transcription units in post-natal day 14
918 oocytes are enriched in TATA-like elements and are sharp. **a, b** Genome-wide A/T-rich
919 dinucleotide (WW) motif analyses of -250/+250 sequences centred on the dominant
920 transcription start sites (TSS, position +1, dashed red line) of TBPL2-dependent (**a**, n =
921 32448) and TBPL2-indendent (**b**, n = 23886) TSS clusters. Sequences have been ordered by
922 increasing size of the interquantile width of each. The red arrowheads indicate the WW
923 enrichment at position -30 in the TBPL2-dependent TSS clusters (**a**) and the equivalent
924 position in the TBPL2-independent TSS clusters (**b**). The number of TSS clusters is indicated
925 in brackets. **c** Distribution of the best TATA box position weight matrix (PWM) matches
926 within a -35 to -20 region upstream of the dominant TSSs (+1) of TBPL2-dependent (blue)
927 compared to the TBPL2-independent (orange) TSS clusters. The dashed lines indicate the
928 median of the TATA box PWM matches for the TBPL2-dependent (blue) and the TBPL2-
929 independent (orange) TSS clusters (*p* value after a two-tailed Wilcoxon rank-sum test). **d, e**
930 Two selected self-organizing map (SOM) groups of the consensus TSS clusters: the down-
931 regulated promoters (blue, **d**) and the up-regulated promoters (red, **e**) groups. **f, g** Sequence

logos of the -35/+5 sequence of the TBPL2-dependent dominant TSSs from the down-regulated promoters (**f**) and of the TBPL2-independent dominant TSSs from the up-regulated promoters (**g**). **h** Distribution of the best TATA box PWM matches within a -35 to -20 region upstream of the TBPL2-dependent (blue) and TBPL2-independent (orange) mammalian apparent LTR retrotransposons (MaLR) endogenous retroviral elements (ERV) dominant TSS. The dashed lines indicate the median of the TATA box PWM matches for the TBPL2-dependent (blue) and the TBPL2-independent (orange) TSS clusters (*p* value after a two-tailed Wilcoxon rank-sum test). **i, j** Sequence logo of the -35/+5 sequence of the MaLR ERVs TBPL2-dependent (**i**) and TBPL2-independent (**j**) dominant TSSs.

Fig. 6 Shifting promoters. **a, b** Analysis of the TBPL2-dependent versus TBPL2-independent shifting promoters within a -250/+250 region centred on the position of the TBPL2-independent transcription start sites (TSS) clusters (position +1 in (**a, b**) and red dashed line in (**b**)). Position of the TBPL2-dependent (blue) and of the TBPL2-independent (orange) dominant TSSs for each shifting promoter sequence (**a**) and WW dinucleotide enrichment heat map (**l**) from the same set of sequences ordered as in (**b**). **c** Distribution of the best TATA box PWM matches within a -35 to -20 region upstream of the TBPL2-dependent (blue) and TBPL2-independent (orange) dominant TSS of the shifting promoters. The dashed lines indicate the median of the TATA box PWM matches for the TBPL2-dependent (blue) and the TBPL2-independent (orange) shifting TSS clusters (*p* value after a two-tailed Wilcoxon rank-sum test).

Fig. 7 Transcriptome overhaul controlled by TBPL2/TFIIA during oocyte growth. At the beginning of oocyte growth, the transcriptome in primordial and early primary follicles (blue cell) depends on TFIID/TBP (blue complex) transcription from broad promoters (blue line).

957 As TBP protein disappears, Pol II transcription initiation is mediated (red line) only by the
958 oocyte-specific TFIIA/TBPL2 complex (red complex) from sharp promoters. At the growing
959 oocyte stage (red cell) TFIIA/TBPL2 complex is responsible for initiating high levels of Pol II
960 transcription, such as mammalian apparent LTR retrotransposons (MaLR) endogenous
961 retroviral elements (ERV) expression and also expression of genes of which the gene products
962 survey/limit the stability and/or translatability of transcripts previously deposited by
963 TFIID/TBP-dependent Pol II transcription.
964
965

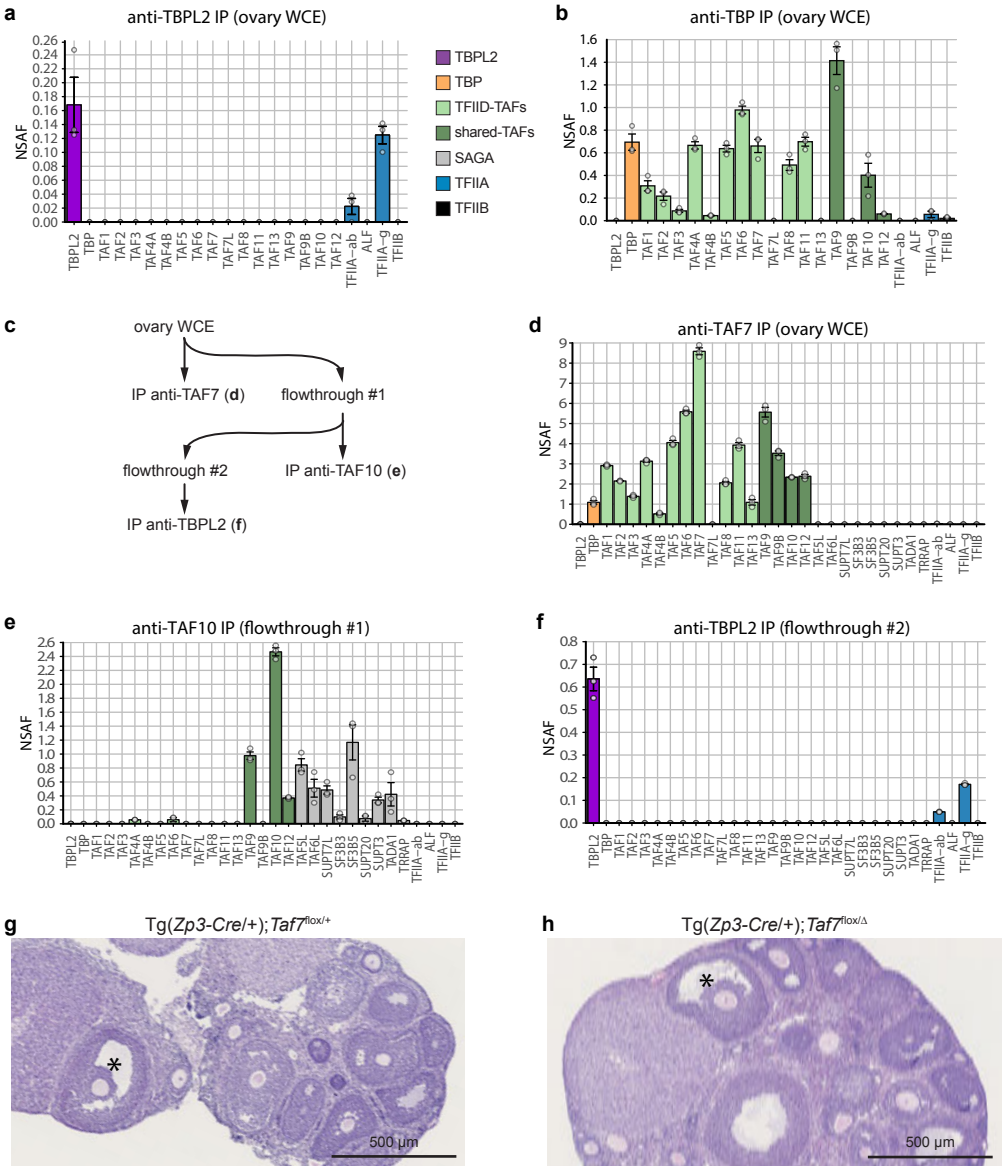
a
anti-TBPL2 IP (ovary WCE)
NSAF
TBPL2
TBP
TFIID-TAFs
shared-TAFs
SAGA
TFIIA
TFIIB
b
anti-TBP IP (ovary WCE)
c
ovary WCE
IP anti-TAF7 (d)
flowthrough #1
flowthrough #2
IP anti-TAF10 (e)
IP anti-TBPL2 (f)
d
anti-TAF7 IP (ovary WCE)
e
anti-TAF10 IP (flowthrough #1)
f
anti-TBPL2 IP (flowthrough #2)
g
Tg(Zp3-Cre/+);Taf7flox/+
h
Tg(Zp3-Cre/+);Taf7flox/Δ
500 µm

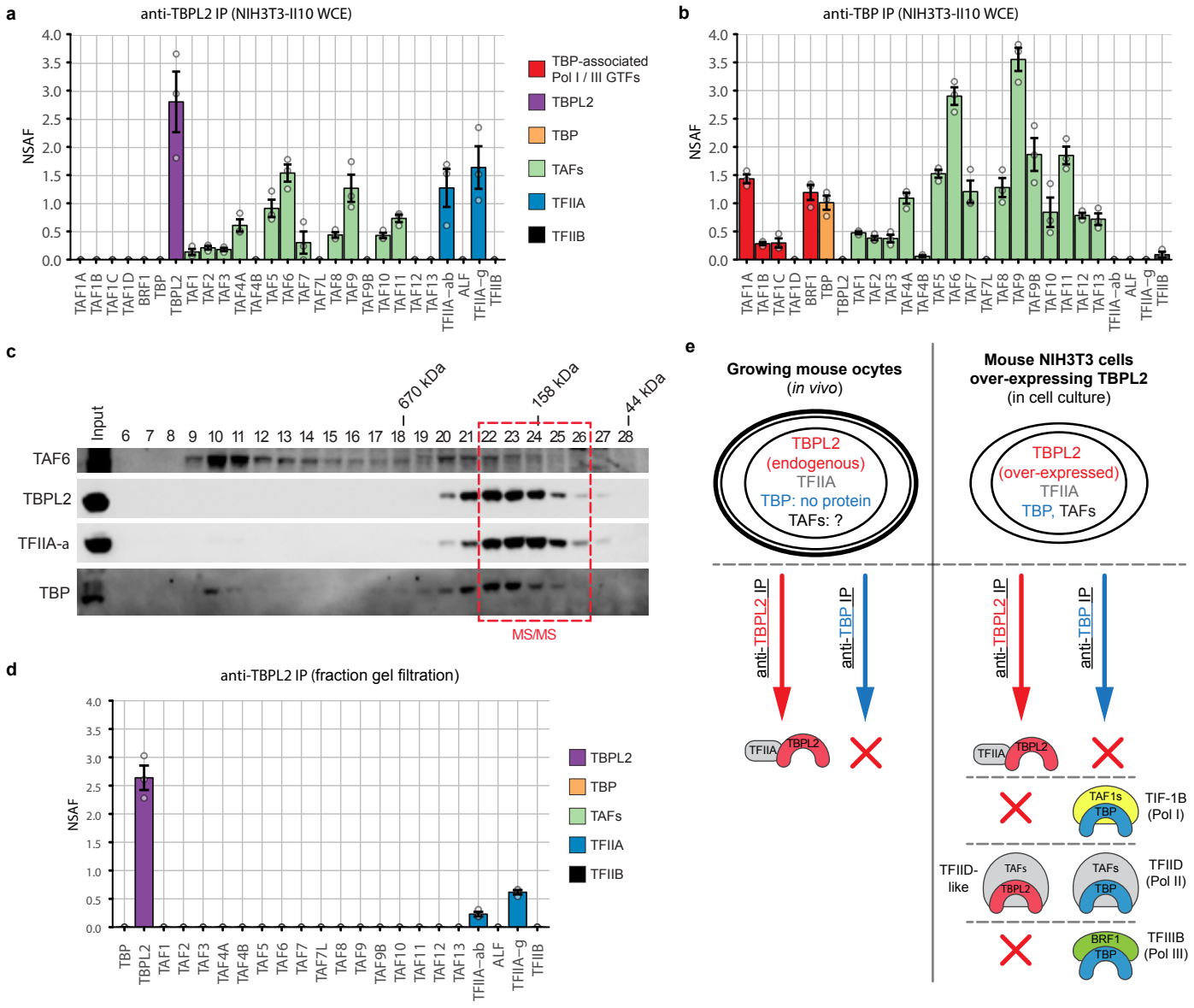
a
anti-TBPL2 IP (NIH3T3-II10 WCE)
NSAF
TBP-associated Pol I / III GTFs
TBPL2
TBP
TAFs
TFIIA
TFIIB
b
anti-TBP IP (NIH3T3-II10 WCE)
c
670 kDa
158 kDa
44 kDa
Input
TAF6
TBPL2
TFIIA-a
TBP
MS/MS
d
anti-TBPL2 IP (fraction gel filtration)
e
Growing mouse ocytes
(in vivo)
TBPL2
(endogenous)
TFIIA
TBP: no protein
TAFs: ?
Mouse NIH3T3 cells
over-expressing TBPL2
(in cell culture)
TBPL2
(over-expressed)
TFIIA
TBP, TAFs
anti-TBPL2 IP
anti-TBP IP
TFIIA
TBPL2
TAF1s
TBP
TIF-1B
(Pol I)
TFIID-
like
TAFs
TBPL2
TAFs
TBP
TFIID
(Pol II)
BRF1
TBP
TFIIIB
(Pol III)

Fig. 2

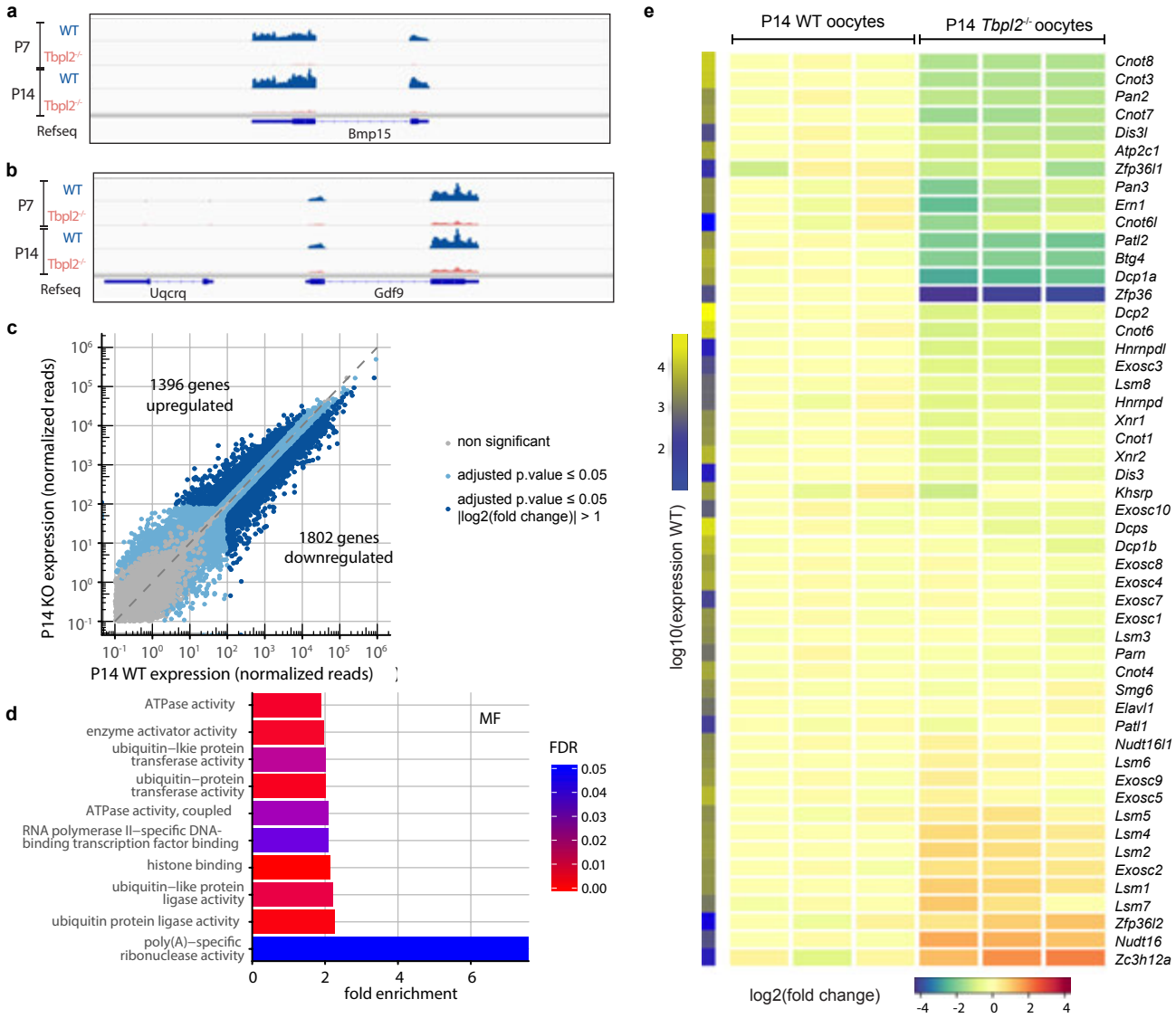
a
P7
WT
Tbpl2-/-
P14
WT
Tbpl2-/-
Refseq
Bmp15
b
P7
WT
Tbpl2-/-
P14
WT
Tbpl2-/-
Refseq
Uqcrq
Gdf9
c
1396 genes upregulated
1802 genes downregulated
non significant
adjusted p.value ≤ 0.05
adjusted p.value ≤ 0.05 |log2(fold change)| > 1
P14 KO expression (normalized reads)
P14 WT expression (normalized reads)
d
MF
ATPase activity
enzyme activator activity
ubiquitin–like protein transferase activity
ubiquitin–protein transferase activity
ATPase activity, coupled
RNA polymerase II–specific DNA-binding transcription factor binding
histone binding
ubiquitin–like protein ligase activity
ubiquitin protein ligase activity
poly(A)–specific ribonuclease activity
fold enrichment
FDR
0.05
0.04
0.03
0.02
0.01
0.00
e
P14 WT oocytes
P14 Tbpl2-/- oocytes
log10(expression WT)
Cnot8
Cnot3
Pan2
Cnot7
Dis3l
Atp2c1
Zfp36l1
Pan3
Ern1
Cnot6l
Patl2
Btg4
Dcp1a
Zfp36
Dcp2
Cnot6
Hnrnpdl
Exosc3
Lsm8
Hnrnpd
Xrn1
Cnot1
Xrn2
Dis3
Khsrp
Exosc10
Dcps
Dcp1b
Exosc8
Exosc4
Exosc7
Exosc1
Lsm3
Parn
Cnot4
Smg6
Elavl1
Patl1
Nudt16l1
Lsm6
Exosc9
Exosc5
Lsm5
Lsm4
Lsm2
Exosc2
Lsm1
Lsm7
Zfp36l2
Nudt16
Zc3h12a
log2(fold change)

Fig. 3

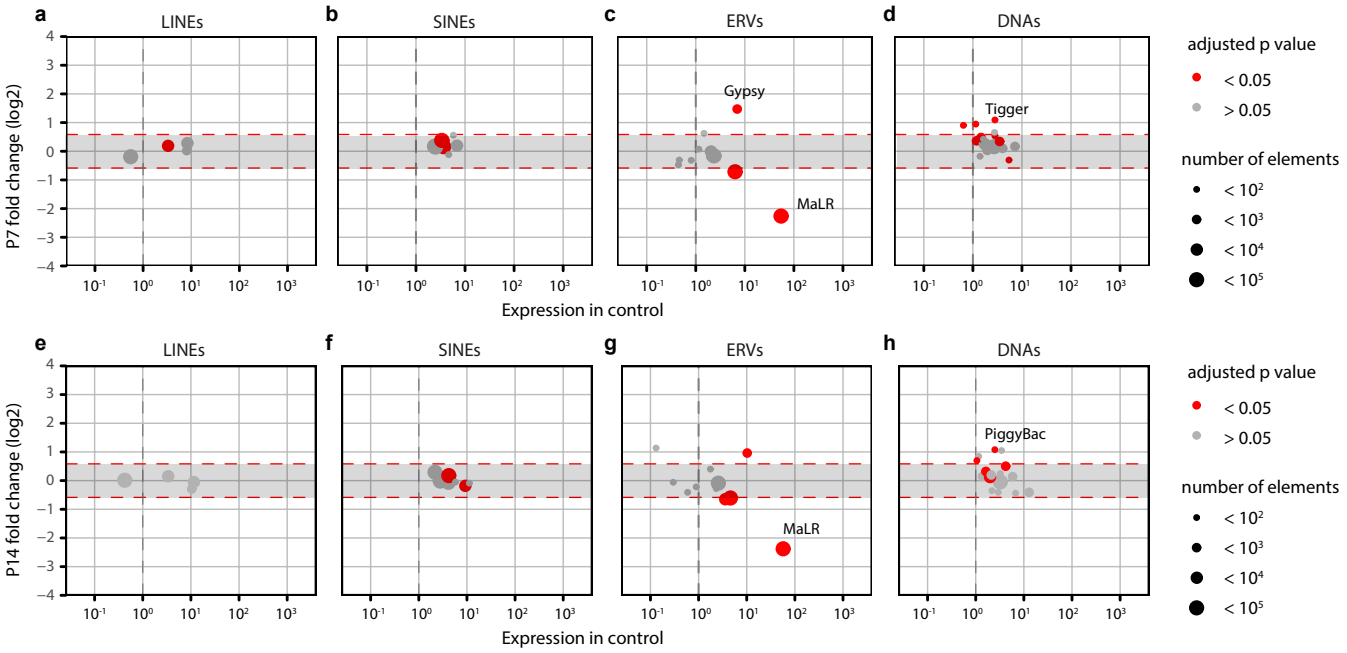
a
LINEs
b
SINEs
c
ERVs
d
DNAs
Gypsy
Tigger
MaLR
P7 fold change (log2)
Expression in control
adjusted p value
< 0.05
> 0.05
number of elements
< 10²
< 10³
< 10⁴
< 10⁵
e
LINEs
f
SINEs
g
ERVs
h
DNAs
PiggyBac
MaLR
P14 fold change (log2)
Expression in control
adjusted p value
< 0.05
> 0.05
number of elements
< 10²
< 10³
< 10⁴
< 10⁵

Fig. 4

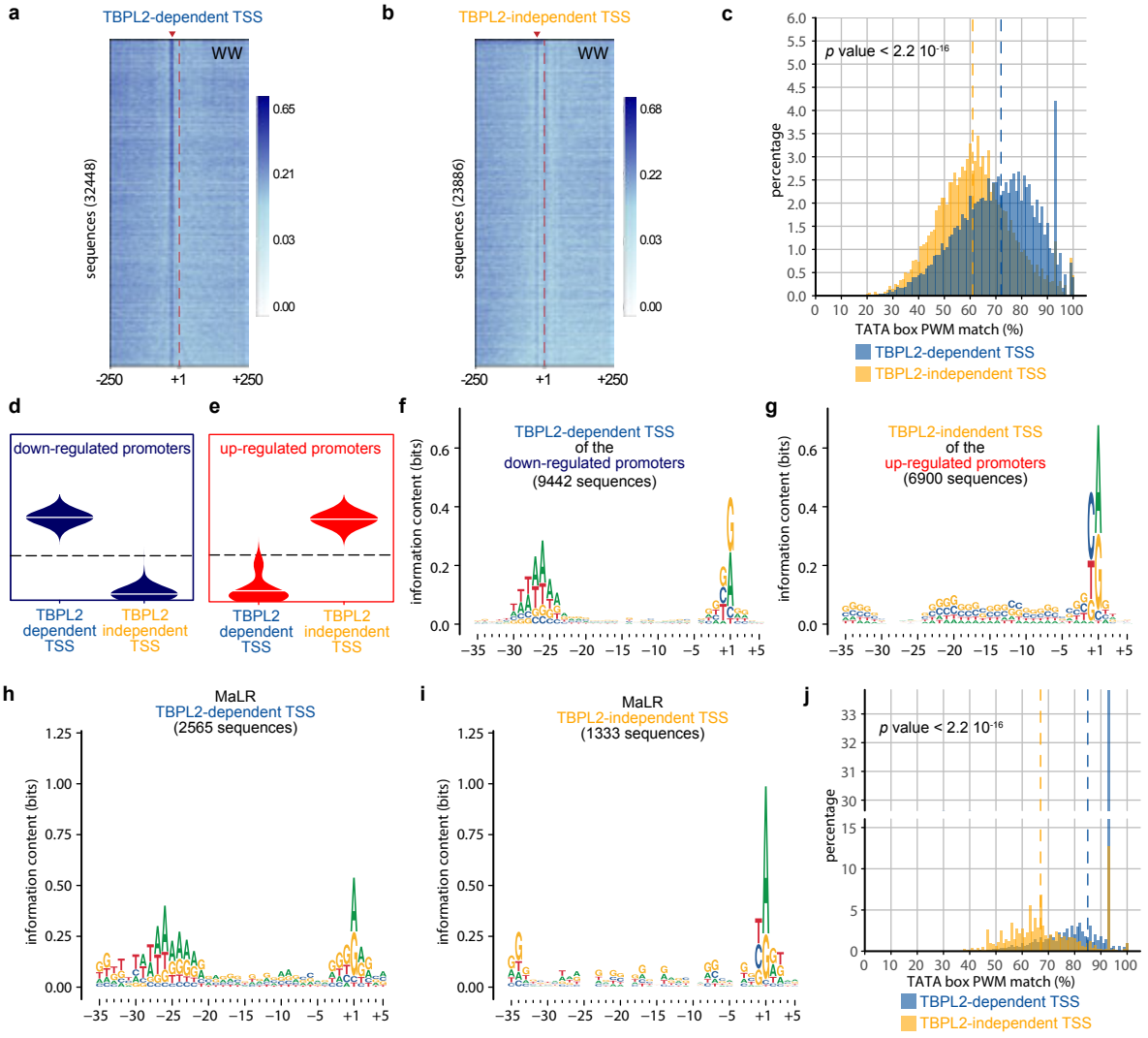
a
TBPL2-dependent TSS
WW
sequences (32448)
0.65
0.21
0.03
0.00
-250
+1
+250
b
TBPL2-independent TSS
WW
sequences (23886)
0.68
0.22
0.03
0.00
-250
+1
+250
c
p value < 2.2 10-16
percentage
TATA box PWM match (%)
TBPL2-dependent TSS
TBPL2-independent TSS
d
down-regulated promoters
TBPL2 dependent TSS
TBPL2 independent TSS
e
up-regulated promoters
TBPL2 dependent TSS
TBPL2 independent TSS
f
TBPL2-dependent TSS of the down-regulated promoters (9442 sequences)
information content (bits)
g
TBPL2-indendent TSS of the up-regulated promoters (6900 sequences)
information content (bits)
h
MaLR
TBPL2-dependent TSS
(2565 sequences)
information content (bits)
i
MaLR
TBPL2-independent TSS
(1333 sequences)
information content (bits)
j
p value < 2.2 10-16
percentage
TATA box PWM match (%)
TBPL2-dependent TSS
TBPL2-independent TSS

Fig. 5

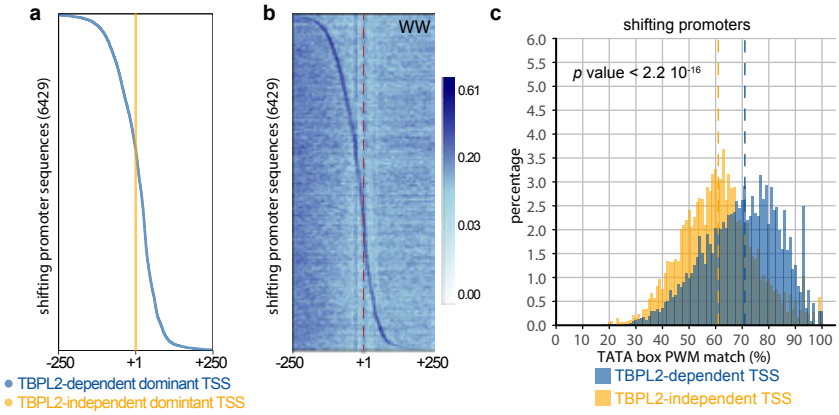
a
shifting promoter sequences (6429)
-250
+1
+250
TBPL2-dependent dominant TSS
TBPL2-independent domintant TSS
b
WW
shifting promoter sequences (6429)
-250
+1
+250
0.61
0.20
0.03
0.00
c
shifting promoters
p value < 2.2 10-16
percentage
TATA box PWM match (%)
TBPL2-dependent TSS
TBPL2-independent TSS

Fig. 6

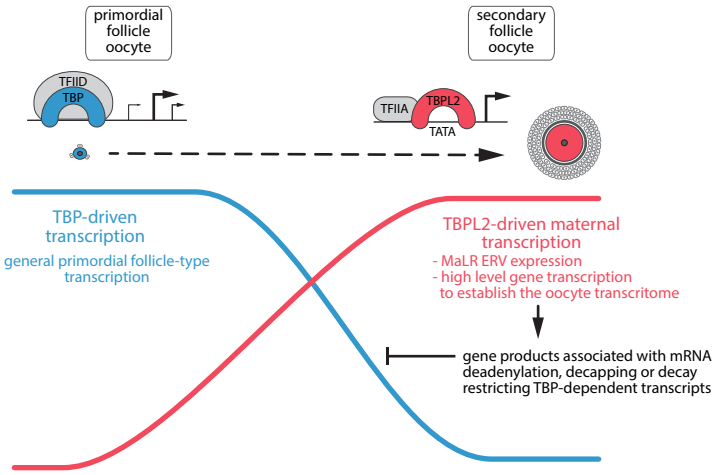
primordial follicle oocyte
secondary follicle oocyte
TFIID
TBP
TFIIA
TBPL2
TATA
TBP-driven transcription
general primordial follicle-type transcription
TBPL2-driven maternal transcription
- MaLR ERV expression
- high level gene transcription to establish the oocyte transcritome
gene products associated with mRNA deadenylation, decapping or decay restricting TBP-dependent transcripts

Fig. 7